octahedral site, indicating a scenario in which V^{III} is in the octahedral VS_6 site and V^{V} is in the tetragonal VSO_3 site.

To confirm this mixed-valence state, they simulated the experimental spectrum of $Ba_3V_2S_4O_3$ with the well proven full-multiplet configuration-interaction approach (red line) using XTLS 8.3 code for three coordinations: (a) V^{III} in octahedral $V^{III}S_6$ site, V^{V} in tetragonal $V^{V}O_3S$ site, (b) V^{V} in octahedral $V^{V}S_6$ site and V^{III} in tetragonal $V^{III}O_3S$ site, and (c) both sites V^{IV}. Figure 3(a) shows a satisfactory agreement between the experimental spectrum (black line) and the theoretical simulation (red line). For $V^{V}S_6$ and $V^{III}O_3S$, Figure 3(b) shows a disagreement of overall spectral features of the experimental and simulated data, especially the lower-energy double signals about 513.1 and 513.6 eV originating from the V^{III} ion in the octahedral site. The possibility that both octahedral and tetrahedral sites have V^{IV} can also be excluded because of the disagreement of spectral features and the overall peak shape between the experimental results and simulation, shown in Fig. 3(c). These results clearly confirm the coordination $V^{III}S_6$ and $V^{V}O_3S$, a perfect example of charge disproportionation according to the HSAB rule; VIII is found purely with sulfur, that is, a soft anion, whereas the harder anion oxygen coordinates only to V^{V}. From the XAS, $Ba_3V_2S_4O_3$ contains one magnetic vanadium ion, V^{III} (d^2, $S = 1$), and one diamagnetic V^{V} (d^0, $S = 0$) per formula unit. The expected spin-only moment for a species with $S = 1$ is 2.83 μ_B, which is near the value 2.77 μ_B estimated from a Curie-Weiss fit of $\chi^{-1}(T)$ data.

Hopkins *et al.* synthesized a single-phase $Ba_3V_2S_4O_3$ powder, and investigated its physical properties. They clarified that vanadium in $Ba_3V_2S_4O_3$ takes charge-disproportionated $V^{III}S_6$ and $V^{V}SO_3$ coordination through analysis of XAS, which means that $Ba_3V_2S_4O_3$ is Mott insulating with $S = 1$. (Reported by Jun Okamoto)

This report features the work of Emily J. Hopkins, Zhiwei Hu, Liu Hao Tjeng and their co-workers published in Chem.-Eur. J. ***21****, 7938 (2015).*

References

1. C. Blumenstein, J. Schäffer, S. Mietke, S. Meyer, A. Dollinger, M. Lochner, X. Y. Cui, L. Patthey, R. Matzdorf, and R. Claessen, Nature Phys. **7**, 776 (2011).
2. F. Calvagna, J. Zhang, S. Li, and C. Zheng, Chem. Mater. **13**, 304 (2001).
3. M. Nakamura, A. Sekiyama, H. Namatame, and A. Fujimori, Phys. Rev. B **49**, 16191 (1994).
4. I. Affeck, J. Phys. Condens. Matter **1**, 3047 (1989).
5. F. D. M. Haldane, Phys. Rev. Lett. **45**, 1358 (1980).
6. B. J. Hopkins, Y. Prots, U. Burkhardt, Y. Watier, Z. Hu, C. Y. Kuo, J.-C. Chiang, T.-W. Pi, A. Tanaka, L.-H. Tjeng, and M. Valldor, Chem. Eur. J. **21**, 7983 (2015).

Three-Dimensional Dirac Semimetal

Topological insulators (TI) are new quantum materials characterized with a bulk insulating gap and gapless surface states protected by time-reversal symmetry, which is realized by band inversion induced by spin-orbit coupling with an odd number of Dirac cones. The topological classification of materials has recently been extended to a higher dimension in the so-called three-dimensional topological Dirac semimetal (TDS) phase. In contrast to TI, the TDS phase exhibits linear dispersion in all three dimensions and is protected by the crystalline symmetry. A TDS phase was predicted theoretically in Na_3Bi and Cd_3As_2 materials and confirmed experimentally using angle-resolved photoemission spectroscopy (ARPES). These TDS phases might, notably, be a 3D-Dirac semimetal of a new type due to the lack of inversion symmetry, which causes the lifting of the spin degeneracy of certain bands in the vicinity of the Dirac point, thereby raising the possibility of realizing the Weyl semimetal phase. The 3D Dirac semimetal has thus attracted much attention in physics and material science. The conduction and valence bands of Cd_3As_2 touch at the Dirac nodes in the bulk band structure, which gives rise to bulk Dirac fermions featuring robust topologically protected linear dispersion in 3D. In 2015, a research team of Fang-Cheng Chou (National Taiwan University) demonstrated a method of growth to obtain large plate-like single crystals of Cd_3As_2 and performed various characterizations on a Cd_3As_2 single crystal to reveal its unique functionalities.

In their work, they presented a detailed report on the self-selecting vapor growth technique of the crystal growth and the characterization of large and high-quality single crystals of Cd_3As_2. In particular, they generated crystals containing self-selected large facets of two types, namely the (112) and (even 00) orientations. Figure 1 shows the X-ray diffraction pattern of the sample as grown and the refined synchrotron X-ray diffraction pattern recorded at **BL01C2**. All diffraction signals can be indexed with space group I41cd. A Rietveld refinement on the XRD pattern yields lattice parameters $a = 12.6512(3)$ Å and $c = 25.4435(4)$ Å. The crystal structure of Cd_3As_2 has been shown to be complicated, depending strongly on the temperature of growth and the rate of quenching. Two space groups have been assigned to the

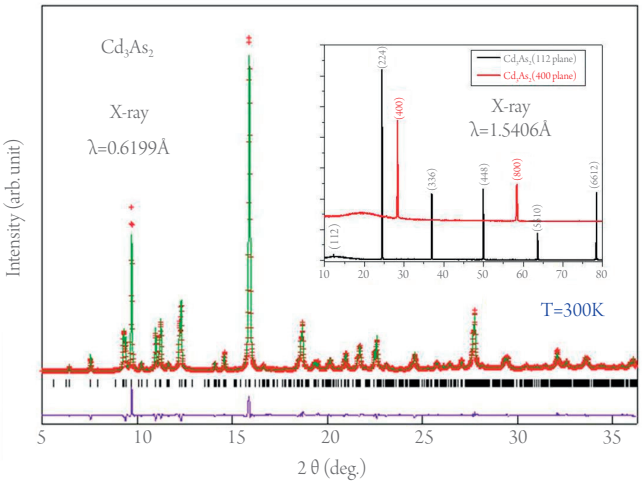

Fig. 1: Powder X-ray diffraction pattern of a Cd_3As_2 sample (red crosses) and its Rietveld refinement (green curve). The inset shows the obtained diffraction patterns of single crystals with facets of preferred orientations along directions (112) and (even 00).

crystals obtained with slow cooling: non-centrosymmetric I41cd and I41/acd with centrosymmetry. The I41cd and I41/acd symmetry difference is a reflection of the varied ordering type of $CdAs_4$ tetrahedral units packed in a large unit cell of stacked fluorite-like structure with vacancies. The Cd_3As_2 crystal structure studied in this work can be satisfactorily indexed with space group I41cd.

The band structure of the grown Cd_3As_2 single crystal was characterized with ARPES measurements at beam line 4.0.3 at Advanced Light Source in Berkeley, California. Sharp XPS signals at binding energies EB~11 and 41 eV that correspond to cadmium 4d and arsenic 3d core levels were observed, confirming the chemical composition of the Cd_3As_2 single crystal to be correct. Remarkably, a low-lying small feature that crossed the Fermi level was observed, which corresponds to surface bands of Cd_3As_2. The linearly dispersive upper Dirac cone is notably located at the surface Brillouin zone center; the Dirac point is found at binding energy 200 meV. The spectral characterization shows a linear dispersive band, thus confirming the high quality of the sample. The surface structure of the vacuum-cleaved Cd_3As_2 surface was further explored with STM measurements. The observed pseudo-hexagonal nearest-neighbor lattice spacing 0.435 nm is near that expected for the (112) surface. Tunneling spectra were subsequently recorded for this (112) surface. The results reveal a conductance minimum at approximately 200 meV below the Fermi level, consistent with the energy of the Dirac point observed in the ARPES data. The approximately linear increase in conductance above this point is consistent also with the linearly dispersive upper Dirac cone observed using ARPES. Resistivity data were measured using a standard four-probe method. The temperature dependence of the resistivity shows that metallic behavior is observed in Cd_3As_2 crystals. The resistivity is nearly independent of temperature below $T = 5$ K, giving a residual resistivity in the range approximately 0.2–0.4 mΩ cm. The Hall resistivity is practically linear under a magnetic field up to 15 T with the Shubnikov-de Haas oscillation appearing at higher fields.

Their work delivers large plate-like high- quality single crystals of Cd_3As_2 with large facets of (112) and (even 00) planes prepared with a self-selecting vapor growth method. The combination of ARPES, STM and transport measurements revealed the unique band structure of 3D Dirac semimetal Cd_3As_2. (Reported by Ying-Hao Chu)

This report features the work of Fang-Cheng Chou and his co-workers published in Sci. Rep. **5**, *12966 (2015).*

Reference

1. R. Sankar, M. Neupane, S.-Y. Xu, C. J. Butler, I. Zeljkovic, I. P. Muthuselvam, F.-T. Huang, S.-T. Guo, Sunil K. Karna, M.-W. Chu, W. L. Lee, M.-T. Lin, R. Jayavel, V. Madhavan, M. Z. Hasan, and F. C. Chou, Sci. Rep. **5**, 12966 (2015).

Interlayer Coupling Affects the Growth of 2D Stripe Orders

Doped Mott insulators have served as a rich playground for strongly correlated electron systems, but the physics is incompletely comprehended. The complication results from an interplay between competing orders, such as charge, spin, orbital and lattice, and strong quantum fluctuations.[1] In high-T_C superconductor $La_{2-x}Sr_xCuO_4$ (LSCO), in which holes are doped into the antiferromagnetic (AFM) Mott insulating La_2CuO_4, unidirectional self-organized electronic stripes are induced in plane $a \times b$ of the crystal space.[2] This intralayer coupling between the ordered charges and spins has been widely discussed; it is natural to ask what role the interlayer coupling between the charge and spin orders in separate planes plays in these systems.

$La_{2-x}Sr_xNiO_4$ (LSNO) has a tetragonal structure, shown in Fig. 1(a), and is isostructural with the superconducting cuprate LSCO. Both LSCO and LSNO are AFM Mott insulators in the absence of hole doping. While LSCO becomes a high-T_C superconductor with hole doping to a small extent, LSNO remains insulating for doping levels up to 90 %.[3] LSNO, however, shows an alternating pattern of AFM domains (spin stripes) separated by charge stripes within each two-dimensional NiO layer, shown in Fig. 1(b);[4] the stripes lead to charge and spin satellite reflections with wave vectors $Q_{CO} = (H \pm 2\varepsilon, 0, L_1)$ and $Q_{SO} = (H \pm \varepsilon, 0, L_2)$, in which H and L_2 are integers, L_1 is odd and ε is determined by the hole concentration with $\varepsilon \sim x$. For

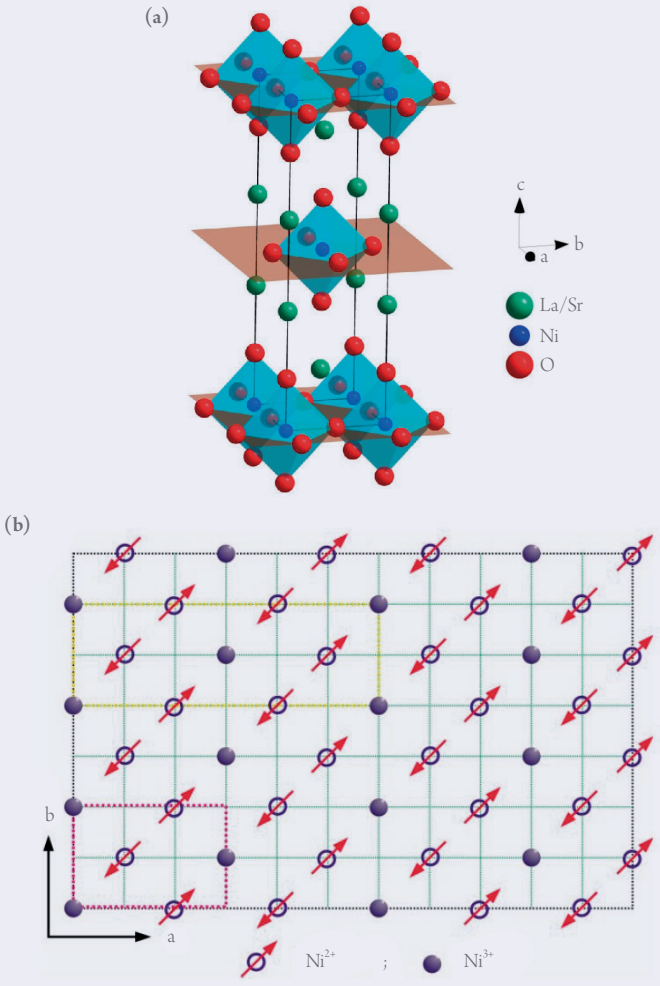

Fig. 1: (a) Crystal structure of LSNO. (b) Schematic view of charge and spin stripes in LSNO in NiO_2 planes. The arrows represent Ni^{2+} ions and solid circles are the holes. Yellow and red boxes indicate the size of spin and charge modulations. [Reproduced from Ref. 5]